

First-principles study of ground state properties and high pressure behavior of  $\text{ThO}_2$ Baotian Wang<sup>1,2</sup>, Hongliang Shi<sup>2,3</sup>, Weidong Li<sup>1</sup>, and Ping Zhang<sup>2</sup><sup>1</sup>Institute of Theoretical Physics and Department of Physics,

Shanxi University, Taiyuan 030006, People's Republic of China

<sup>2</sup>LCP, Institute of Applied Physics and Computational Mathematics, Beijing 100088, People's Republic of China<sup>3</sup>SKLSP, Institute of Semiconductors, Chinese Academy of Sciences, People's Republic of China

The mechanical properties, electronic structure and phonon dispersion of ground state  $\text{ThO}_2$  as well as the structure behavior up to 240 GPa are studied by using first-principles density-functional theory. Our calculated elastic constants indicate that both the ground state fluorite structure and high pressure cotunnite structure of  $\text{ThO}_2$  are mechanically stable. The bulk modulus, shear modulus, and Young's modulus of cotunnite  $\text{ThO}_2$  are all smaller by approximately 25% compared with those of fluorite  $\text{ThO}_2$ . The Poisson's ratios of both structures are approximately equal to 0.3 and the hardness of fluorite  $\text{ThO}_2$  is 27.33 GPa. The electronic structure and bonding nature of fluorite  $\text{ThO}_2$  are fully analyzed, which show that the Th-O bond displays a mixed ionic/covalent character. The valence of Th and O ions in fluorite  $\text{ThO}_2$  can be represented as  $\text{Th}^{3.834+}$  and  $\text{O}^{0.452-}$ . The phase transition from the fluorite to cotunnite structure is calculated to be at the pressure of 26.5 GPa, consistent with recent experimental measurement by Idiri et al. [1]. For the cotunnite phase it is further predicted that an isostructural transition takes place in the pressure region of 80 to 130 GPa.

PACS numbers: 61.50.Ah, 61.50.Ks, 71.15.Mb, 63.20.dk

## I. INTRODUCTION

Besides uranium and plutonium, thorium is also one kind of important nuclear materials. Metal thorium and its compounds have been widely investigated both experimentally and theoretically since metal thorium was found in 1828. Among thorium compounds, thorium dioxide  $\text{ThO}_2$ , which is a stable diamagnetic transparent insulating solid, has attracted special attention. In addition to its usage as an important nuclear fuel material, thorium dioxide has also been used as a solid-state electrolyte. In particular, due to its prominent hardness,  $\text{ThO}_2$  has potential interests as an optical component material and laser host.

Recently, there has occurred in the literature a series of experimental reports on pressure-induced phase transition of  $\text{ThO}_2$  [1, 2, 3]. At ambient pressure,  $\text{ThO}_2$  crystallizes in the (CaF<sub>2</sub>-type) fluorite structure with space group Fm $\bar{3}$ m (No. 225). By using the energy dispersive x-ray diffraction (EDXRD) method, Dancusse et al. [3] reported that at 40 GPa,  $\text{ThO}_2$  undergo a phase transition to an orthorhombic structure of cotunnite (Pbc<sub>2</sub>) type with space group Pnma (No. 62). Later, through improving experimental measurement technique, Idiri et al. [1] observed that this phase transition really begins around 30 GPa, and the two phases coexist in a wide pressure range of nearly 20 GPa. Additional high-pressure Raman spectroscopy measured by Jayaraman et al. [2] also suggested that  $\text{ThO}_2$  starts to transform into the cotunnite structure around 30 GPa.

In contrast to the above-mentioned extensive experi-

mental investigation, a systematic theoretical study on the phase transition of  $\text{ThO}_2$  at high pressure is still lacking. In particular, considering the obvious discrepancy between two experimental groups [1, 3] involving the transition pressure, such a theoretical investigation from basis quantum mechanics is not only complementary but also indispensable. Motivated by this observation, in this paper, we present a first-principles study by calculating the total energies and enthalpies of  $\text{ThO}_2$  at its experimentally established crystalline phases. Our calculation shows that the transition pressure is around 30 GPa, consistent with the recent experiment by Idiri et al. [1].

The other task for this paper is to theoretically present a thorough description of physical, mechanical and chemical bonding properties of  $\text{ThO}_2$  at its ground state of the fluorite phase. To date, theoretical studies of the ground-state behavior of  $\text{ThO}_2$  are very scarce in literature [4, 5, 6, 7, 8] and some of them are even inconsistent with the experimental data to a large extent. For example, without taking into account the 5f state, Kelly et al. [4] calculated the bulk modulus  $B$  of  $\text{ThO}_2$  to be 290 GPa, which is far from the experimental value of 198 GPa. On the other hand, based on a purely ionic model, Harding et al. [5] obtained  $B = 175$  GPa, which, compared to the experimental data, clearly underestimate the binding interaction in the material to a large extent. This as a whole encourages us to theoretically report a systematic investigation on the ground-state properties of  $\text{ThO}_2$  at its ambient phase. Besides the consistency with the existing experimental data, we expect that the new results for the first time predicted in this paper and experimentally inaccessible at present, such as the hardness, the phonon spectrum, and the charge transfer of the Th-O bond, will be of great help for a primary understanding

---

Electronic address: zhang.ping@iapcm.ac.cn

of  $\text{ThO}_2$ . The rest of this paper is arranged as follows. In Sec. II the computational method is briefly described. In Sec. III and Sec. IV we present our calculated results, some of which are made comparison with available experimental and theoretical results. In Sec. V we summarize the conclusions of this work.

## II. COMPUTATIONAL METHOD

Our total energy calculations are carried out by employing the plane-wave basis pseudopotential method as implemented in Vienna ab initio simulation package (VASP) [9]. The exchange and correlation effects are described by the DFT within the generalized gradient approximation (GGA) [10]. The electron and core interactions are included using the frozen-core projected augmented wave (PAW) approach which combines the accuracy of augmented-plane-wave methods with the efficiency of the pseudo-potential approach [11]. The thorium  $6s^2 7s^2 6p^6 6d^1 5f^1$  and the oxygen  $2s^2 2p^4$  electrons are treated as valence electrons. Note that although the 5f state are empty in elemental Th, this level turns to evolve into a hybridization with O 2p state in the valence band, as well as to prominently contributes to the conduction band (see Fig. 3 below). We use a  $9 \times 9 \times 9$  k-point grid with Monkhorst-Pack scheme [12] for fluorite  $\text{ThO}_2$  and  $9 \times 15 \times 9$  k-point grid for cotunnite structure. Electron wave function is expanded in plane waves up to a cutoff energy of 500 eV, and all atoms are fully relaxed until the quantum mechanical forces become less than 0.02 eV/Å.

To obtain optimized lattice constants of ground state  $\text{ThO}_2$ , first, we calculate several total energies at different lattice constants around the experimental value. Then we fit the energy-volume data to the third-order Birch-Murnaghan equation of state (EOS) [13] to give the theoretical equilibrium volume, minimum energy, bulk modulus  $B$ , and pressure derivative of the bulk modulus  $B^0$ . On the other hand, the bulk modulus  $B$ , shear modulus  $G$ , Young's modulus  $E$ , Poisson's ratio  $\nu$ , can also be derived from the elastic constants. We find that the bulk modulus  $B$  obtained by these two ways are in good agreement, indicating that our calculations are self-consistent.

## III. GROUND STATE PROPERTIES FOR FLUORITE-TYPE THORIUM DIOXIDE

### A. Atomic structure and mechanical properties

At ambient condition thorium dioxide crystallize in a  $\text{CaF}_2$ -like ionic structure. Its cubic unit cell is composed of four  $\text{ThO}_2$  formula units with the thorium atoms and the oxygen atoms in 4a and 8c sites, respectively [see Fig. 1(a)]. Each Th atom is surrounded by eight O atoms forming a cube and each O connects with four

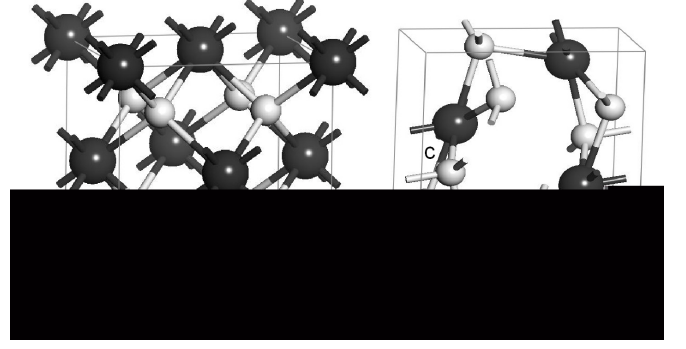


FIG. 1: Cubic unit cell for  $\text{ThO}_2$  in space group  $Fm\bar{3}m$  (a) and orthorhombic unit cell in space group  $Pnm2_1$  (b), larger black spheres stand for Th atoms and the smaller white O.

Th atoms to build a tetragon. A particular feature of this structure is the presence of a large octahedral hole sited at position  $\frac{1}{2}; \frac{1}{2}; \frac{1}{2}$ . The present optimized lattice constant ( $a_0$ ) is 5.62 Å (see Table I), in good agreement with the experimental [1, 6] value of 5.6 Å.

Elastic constants can measure the resistance and mechanical features of crystal to external stress or pressure, thus describing the stability of crystals against elastic deformation. For small strains Hooke's law is valid and the crystal energy  $E$  is a quadratic function of strain [14]. Thus, to obtain the total minimum energy for calculating the elastic constants to second order, a crystal is strained and all the internal parameters relaxed. Consider a symmetric  $3 \times 3$  nonrotating strain tensor  $\epsilon$  which has matrix elements " $\epsilon_{ij}$  ( $i, j = 1, 2, \text{ and } 3$ )" defined by

$$\epsilon_{ij} = \begin{pmatrix} 0 & \epsilon_1 & \epsilon_2 \\ \epsilon_1 & \frac{\epsilon_6}{2} & \frac{\epsilon_5}{2} \\ \epsilon_2 & \frac{\epsilon_5}{2} & \frac{\epsilon_4}{2} \end{pmatrix} \text{Å} : \quad (1)$$

Such a strain transforms the three lattice vectors defining the unstrained Bravais lattice  $\mathbf{a}_k$ ;  $k = 1, 2, \text{ and } 3$  to the strained vectors [15]  $\mathbf{a}_k^0$  as defined by

$$\mathbf{a}_k^0 = (\mathbf{I} + \epsilon) \mathbf{a}_k; \quad (2)$$

where  $\mathbf{I}$  is a unit  $3 \times 3$  matrix. Each lattice vector  $\mathbf{a}_k$  or  $\mathbf{a}_k^0$  is a  $3 \times 1$  matrix. The change in total energy due to above strain (1) is [14]

$$\begin{aligned} E &= E(V; \epsilon_{ij}) - E(V; 0) \\ &= V \sum_{i=1}^3 \sigma_i \epsilon_i + \frac{V}{2} \sum_{i,j=1}^3 C_{ij} \epsilon_i \epsilon_j + O(\epsilon_i^3); \quad (3) \end{aligned}$$

where  $E(V; 0)$  is the total energy for the unstrained crystal,  $\sigma_i$  are the elements of stress tensor, and  $C_{ij}$  are the elastic constants. For cubic structure of  $\text{ThO}_2$ , there are three independent elastic constants, i.e.,  $C_{11}$ ,  $C_{12}$ , and  $C_{44}$ , which are calculated through a proper choice of the set of strains  $\epsilon_i$ ;  $i = 1, \dots, 6$  listed in Table II. In our

TABLE I: Calculated lattice parameter, elastic constants, bulk modulus  $B$ , pressure derivative of the bulk modulus  $B'$ , shear modulus  $G$ , Young's modulus  $E$ , Poisson's ratio  $\nu$ , hardness, and energy band gap ( $E_g$ ) for cubic  $\text{ThO}_2$ . As a comparison, other theoretical works and available experimental data are listed.

Property	This study	Previous calculation	Experiment
	VASP-GGA	FP-LMTO-GGA	
$a_0$ (Å)	5.62	5.61 <sup>a</sup>	5.60001 (3) <sup>b</sup> , 5.598 (3) <sup>d</sup>
$C_{11}$ (GPa)	349.5	376.0 <sup>a</sup>	367 <sup>c</sup>
$C_{12}$ (GPa)	111.4	109.8 <sup>a</sup>	106 <sup>c</sup>
$C_{44}$ (GPa)	70.6	68.1 <sup>a</sup>	79 <sup>c</sup>
$B$ (GPa)	191	198 <sup>a</sup> , 198 <sup>d</sup>	198 (2) <sup>b</sup> , 195 (2) <sup>d</sup>
$B'$	4.5	4.5 <sup>a</sup> , 4.2 <sup>d</sup>	4.6 (3) <sup>b</sup> , 5.4 (2) <sup>d</sup>
$G$ (GPa)	87.1	94.1 <sup>a</sup>	97 <sup>c</sup>
$E$ (GPa)	226.8	243.8 <sup>a</sup>	249 <sup>c</sup>
	0.302	0.295 <sup>a</sup>	0.285 <sup>c</sup>
Hardness (GPa)	27.33		
$E_g$ (eV)	4.673	4.522 <sup>d</sup>	6 <sup>e</sup>

<sup>a</sup> Reference [8], <sup>b</sup> Reference [1], <sup>c</sup> Reference [16], <sup>d</sup> Reference [6], <sup>e</sup> Reference [23].

TABLE II: Three strain combinations in the strain tensor [Eq. (1)] to calculate the three elastic constants of cubic  $\text{ThO}_2$ .

Strain	Parameters (unlisted $e_i = 0$ )	$E/V$ in $O(2)$
1	$e_1 = e_2 = e_3 =$	$\frac{3}{2}(C_{11} + 2C_{12})^2$
2	$e_1 = e_3 =$	$(C_{11} + C_{12})^2$
3	$e_4 = e_5 = e_6 =$	$\frac{3}{2}C_{44}^2$

First-principles calculations, the strain amplitude is varied in steps of 0.006 from  $\epsilon = -0.036$  to 0.036 and the total energies  $E(V; \epsilon)$  at these strain steps are calculated, and then fitted through the strains with the corresponding parabolic equations of  $E = V$  as given in Tables II to yield the required second-order elastic constants. Note that while computing these energies all atoms are allowed to relax with the cell shape and volume fixed by the choice of strains  $\epsilon_i$ . Our calculated elastic constants for the ground-state fluorite structure of  $\text{ThO}_2$  are listed in Table I. As a comparison, previous theoretical results based on the full-potential linear muffin-tin orbital (FP-LMTO) method [8], as well as available experimental data [16] are also presented in Table I. It is clear that our calculated elastic constants are in good agreement with the experimental results.

After obtaining elastic constants, we can calculate bulk and shear moduli from the Voigt-Reuss-Hill (VRH) approximations [17, 18, 19]. The Voigt bounds [17, 20] on the effective bulk modulus  $B_V$  and shear modulus  $G_V$  are

$$B_V = (C_{11} + 2C_{12})/3 \quad (4)$$

and

$$G_V = (C_{11} - C_{12} + 3C_{44})/5 \quad (5)$$

Under Reuss approximation [18], the Reuss bulk modulus

$B_R$  and Reuss shear modulus  $G_R$  are

$$B_R = B_V \quad (6)$$

and

$$G_R = 5(C_{11} - C_{12})C_{44}/[4C_{44} + 3(C_{11} - C_{12})] \quad (7)$$

The bulk modulus  $B$  and shear modulus  $G$ , based on Hill approximation [19], are arithmetic average of Voigt and Reuss elastic modulus, i.e.,  $B = \frac{1}{2}(B_R + B_V)$  and  $G = \frac{1}{2}(G_R + G_V)$ . The Young's modulus  $E$  and Poisson's ratio  $\nu$  for an isotropic material are given by [21]

$$E = \frac{9BG}{3B + G}; \quad (8)$$

and

$$\nu = \frac{3B - 2G}{2(3B + G)}; \quad (9)$$

The calculated results for these moduli and Poisson's ratio for the fluorite  $\text{ThO}_2$  are listed in Table I. Note that we have also calculated the bulk modulus  $B$  by fitting the Murnaghan equation of state. The derived bulk modulus turns out to be exactly the same as that from the above VRH approximation, which again indicates that our calculations are consistent and reliable. For comparison, other theoretical results [6, 8] and available experimental data [1, 6, 16] are also shown in Table I. It can be seen that on the whole, our present results compare well with those previous experimental and FP-LMTO theoretical results. Concerning the Poisson's ratio, it is well known that for the common materials that have much smaller shear moduli compared with the bulk moduli, their Poisson's ratio is close to 1/3. For the present  $\text{ThO}_2$  system, our calculated shear modulus  $G$  is much lower than the bulk modulus  $B$ . Thus, our calculated result of 0.302 for the Poisson's ratio, as well as the derived result of

0.285 according to the experimentally determined elastic constants [16] and using Eq. (9), can be well understood.

Furthermore, hardness is also one fundamental physical quantity when considering the phase stability and mechanical properties. Note that the hardness is important for the applications of  $\text{ThO}_2$  as both nuclear material and optical components. So here we calculate the hardness of  $\text{ThO}_2$  by using the approach raised by Simunek et al. [22]. In the case of two atoms 1 and 2 forming one bond of strength  $s_{12}$  in a unit cell of volume  $V$ , the expression for hardness has the form [22]

$$H = (C = ) b_{12} s_{12} e^{-f_2}; \quad (10)$$

where

$$s_{12} = \frac{P}{(e_1 e_2)} = (n_1 n_2 d_{12}); e_i = Z_i / r_i \quad (11)$$

and

$$f_2 = \left( \frac{e_1 - e_2}{e_1 + e_2} \right)^2 = 1 - \frac{P}{[(e_1 e_2) = (e_1 + e_2)]^2} \quad (12)$$

are the strength and ionicity of the chemical bond, respectively, and  $d_{12}$  is the interatomic distance;  $C = 1550$  and  $\gamma = 4$  are constants. The radius  $r_i$  is chosen to make sure that the sphere centered at atom  $i$  in a crystal contains exactly the valence electronic charge  $Z_i$ . For fluorite structure  $\text{ThO}_2$ ,  $b_{12} = 32$  counts the interatomic bonds between atom  $\text{Th}$  (1) and  $\text{O}$  (2) in the unit cell,  $n_1 = 8$  and  $n_2 = 4$  are coordination numbers of atom  $\text{Th}$  and  $\text{O}$ , respectively,  $r_1 = 1.81$  (Å) and  $r_2 = 1.00$  (Å) are the atomic radii for  $\text{Th}$  and  $\text{O}$  atoms, respectively,  $Z_1 = 12$  and  $Z_2 = 6$  are valence charge for  $\text{Th}$  and  $\text{O}$  atoms, respectively,  $d_{12} = 2.43$  (Å) is the interatomic distance, and  $V = 145.53$  (Å<sup>3</sup>) is the volume of unit cell. Using Eqs. (10)–(12), we obtain  $s_{12} = 0.081$  and  $f_2 = 0.0025$ . The hardness of  $\text{ThO}_2$  at its ground-state fluorite structure is thus given by  $H = 27.3$  (GPa). This indicates that the fluorite  $\text{ThO}_2$  is a hard material and approaches to a superhard material (hardness > 40 GPa). The high hardness of this crystal can be understood from the dense crystal structure, which results in high valence electron density and short bond distances. The unusual mixture of covalent and ionic components in the  $\text{Th}$ - $\text{O}$  chemical bond will be discussed in the following subsection.

## B. Electronic structure and charge distribution

Almost all the macroscopic properties of materials, such as hardness, elasticity, and conductivity, originate from their electronic structure properties as well as chemical bonding nature. Therefore, it is necessary to perform the electronic structure analysis of  $\text{ThO}_2$ . The calculated band structure (left panel) and total density of states (DOS, right panel) of fluorite  $\text{ThO}_2$  are shown in Fig. 2. The present calculated energy band gap of 4.673 eV

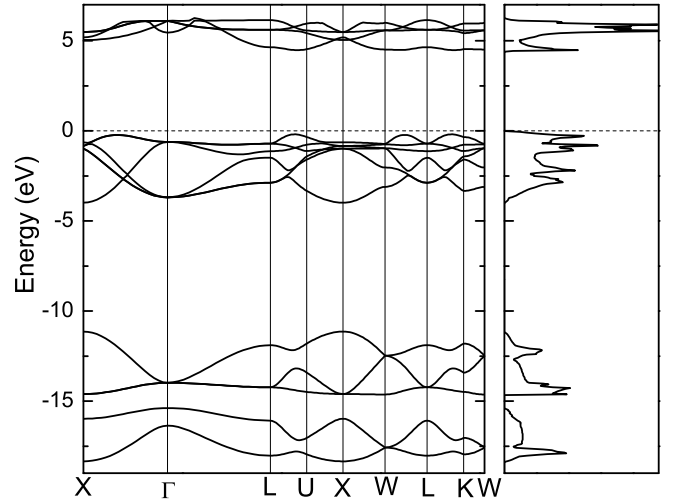


FIG. 2: Band structure (left panel) and total density of states (DOS, right panel) for ground state  $\text{ThO}_2$  with Fermi energy level  $E_F$  taken at 0 eV as shown by the dashed lines.

(listed in Table I), which is consistent with previous FT-LMTO theoretical result of 4.522 eV [6], indicates that  $\text{ThO}_2$  is a typical insulator. The underestimation of band gap compared with experimental value of 6 eV [23] is due to the drawback of the exchange-correlation approximation (GGA). As a comparison, the orbital-resolved partial densities of states (PDOS) for one  $\text{Th}$  atom and two  $\text{O}$  atoms in a unit cell are also presented in Fig. 3. One can see that the low bands covering from -18.33 to -11.22 eV mainly consist of  $\text{O}$  2s and  $\text{Th}$  6p states which shows a clear hybridization. This hybridization is also responsible for the covalency of  $\text{ThO}_2$  (see further discussion below). The high valence bands located just below the Fermi level are mainly contributed by  $\text{O}$  2p states with a little  $\text{Th}$  6d and 5f states and have a band width of 3.79 eV. This illustrates a significant charge transfer from  $\text{Th}$  6d and 5f states to  $\text{O}$  2p states. As for the conduction bands, the DOS is mainly featured by  $\text{Th}$  5f states, mixed with a little  $\text{Th}$  6d and  $\text{O}$  2p states and has a width of 1.78 eV.

In order to gain more insight into the bonding nature of ground state  $\text{ThO}_2$ , we also investigate the valence charge density distribution. The calculated valence charge density map of the (110) plane is plotted in Fig. 4. It is obvious from Fig. 4 that the charge density around  $\text{Th}$  and  $\text{O}$  ions are all near spherical distribution with slightly deformed toward the direction to their nearest neighboring atoms. Furthermore, the charge density around  $\text{Th}$  and  $\text{O}$  ions is high while there is almost no valence charge in the large octahedral-hole interstitial region. This suggests that remarkable ionization exists for thorium and oxygen ions and significant insulating property exhibits in  $\text{ThO}_2$ . In order to describe the ionicity quantitatively and more clearly, we plot in the inset in Fig. 4 the line charge density distribution along the nearest  $\text{Th}$ - $\text{O}$  bond.

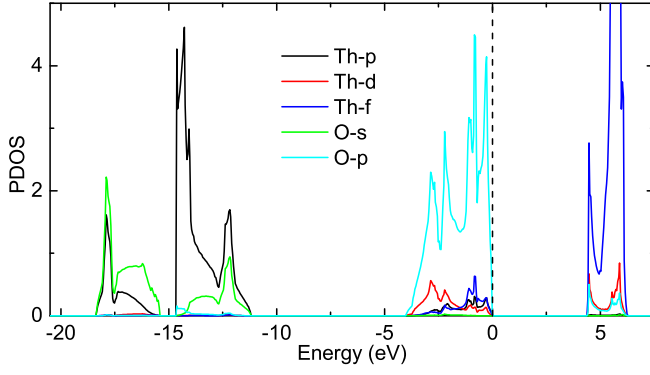


FIG. 3: (Color online) Partial density of states (PDOS) for ground state  $\text{ThO}_2$  at 0 GPa. The Fermi energy level is zero.

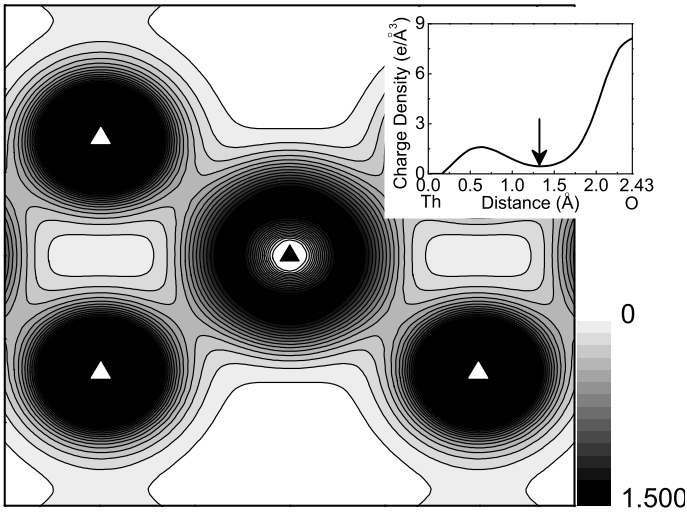


FIG. 4: Valence charge density of  $\text{ThO}_2$  in (110) plane. There N stands for Th, M for O atoms. The contour lines are drawn from 0.0 to 1.5 at 0.1  $\text{e}/\text{\AA}^3$  intervals. The line charge density distribution between Th atom and the nearest neighbor O atom is shown in the inset, where the arrow indicates the minimum value.

Therein the arrow indicates the charge density minimum of  $0.45 \text{ e}/\text{\AA}^3$ . The distance between this charge density minimum point and Th ion is 1.32 Å. According to this, we can define the ionic radius of Th in  $\text{ThO}_2$  as  $r_{\text{Th}} = 1.32 \text{ \AA}$ . After subtracting this value from the Th-O bond length (2.43 Å), one obtains the oxygen ionic radius in  $\text{ThO}_2$  as  $r_{\text{O}} = 1.11 \text{ \AA}$ . The corresponding valency of Th and O in  $\text{ThO}_2$  can be estimated by calculating the valence charges within the spheres of ionic radii. After integration, we find that there are 8.166 electrons around Th and 6.452 electrons around O. As a result, the valency of Th and O can be formally represented as  $\text{Th}^{3.834+}$  and  $\text{O}^{0.452-}$ , respectively. This indicates that the Th and O atoms in  $\text{ThO}_2$  are ionized inequivalently. In other words, Th is ionized almost as  $\text{Th}^{4+}$ , while O is weakly ionized.

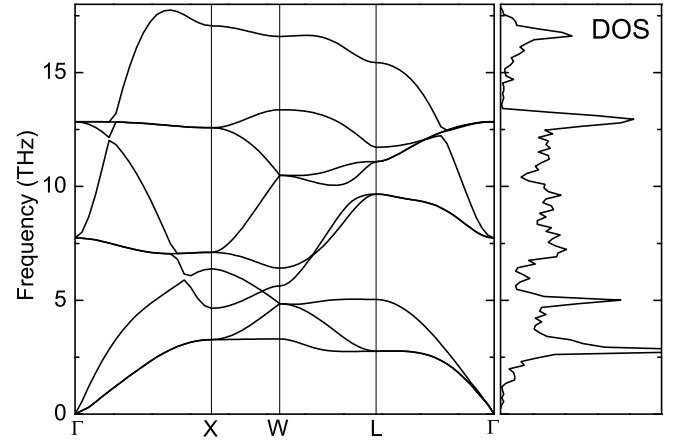


FIG. 5: Calculated phonon dispersion curves along the high-symmetry directions (left panel) and total density of states (DOS, right panel) for ground state  $\text{ThO}_2$ .

This fact, on the other hand, suggests that besides ionicity, the Th-O bond also includes a prominent covalent components, which is consistent with the above PDOS analysis. In fact, the minimum value  $0.45 \text{ e}/\text{\AA}^3$  of charge density along the Th-O bond in  $\text{ThO}_2$  is prominently higher than that in typical ionic crystals. Based on the PDOS and charge density analysis, therefore, we derive that the Th-O bond is a mixture of covalent and ionic components. From this aspect, it is now understandable that the previous full-ionic model [5] has largely underestimated the bulk modulus of  $\text{ThO}_2$ .

### C. Phonon dispersion curve

The calculation of phonon frequencies of the crystalline structure is one of the basic aspects when considering the phase stability, phase transformations, and thermodynamics of crystalline materials. By using the Hellmann-Feynman theorem and the direct method, we have calculated the phonon curves along some high-symmetry directions in the Brillouin zone, together with the phonon density of states. For the phonon dispersion calculation, we use the  $2 \times 2 \times 2$  fcc supercell containing 96 atoms and the  $4 \times 4 \times 4$  Monkhorst-Pack k-point mesh for the Brillouin zone integration. In order to calculate the Hellmann-Feynman forces, we displace four atoms (two Th and two O atoms) from their equilibrium positions and the amplitude of all the displacements is 0.03 Å. The calculated phonon dispersion curves along the  $\Gamma$ -X-W-L- $\Gamma$  directions are displayed in Fig. 5. The  $\Gamma$ -X, X-W, and L- $\Gamma$  lines are along  $\langle 001 \rangle$ ,  $\langle 102 \rangle$ , and  $\langle 111 \rangle$  directions, respectively.

For  $\text{ThO}_2$  in the  $\text{CaF}_2$ -structure primitive cell, there are only three atoms. Therefore, nine phonon modes exist in the dispersion relations. One can see that there is no gap between the optic modes and the acoustic

branches and the LO-TO also has no splitting at  $\Gamma$  point. Due to the fact that thorium is heavier than oxygen atom, the vibration frequency of thorium atom is lower than that of oxygen atom. Therefore, the phonon density of states can be viewed as two parts. One is the part lower than 5.5 THz where the main contribution comes from the thorium sublattice, while the other part higher than 5.5 THz, included both acoustic and optical branches, are dominated by the dynamics of the light oxygen atoms.

#### IV. HIGH PRESSURE BEHAVIOR OF $\text{ThO}_2$

In order to investigate the high pressure behavior of  $\text{ThO}_2$ , we have optimized the structural parameters of its Fm3m and Pnm phases at different pressures by using GGA method. To avoid the Pulay stress problem, we perform the structure relaxation calculations at fixed volumes rather than constant pressures. For Fm3m phase, due to its high symmetry, the structure relaxation calculations are performed at fixed volumes with no relaxation of coordinates. However, for Pnm phase, the coordinates of atoms and the cell shape are necessary to be optimized due to their internal degrees of freedom.

The optimized structural lattice parameters  $a$ ,  $b$ , and  $c$  for the Pnm phase at 0 GPa are 6.174, 3.776, and 7.161 Å, respectively, giving  $V = 167.0 \text{ Å}^3$ . This volume is prominently smaller than the equilibrium volume of 177.5 Å<sup>3</sup> for the Fm3m phase. Using the same method as that has been employed in our previous work on orthorhombic  $\text{BeH}_2$  [24], we have applied the strains and calculated the elastic constants, various moduli, and Poisson's ratio for cotunnite-type  $\text{ThO}_2$  at 0 GPa. The results are collected in Table III. From Table III the following prominent features can be seen: (i) The orthorhombic  $\text{ThO}_2$  at zero pressure is mechanically stable because its elastic constants satisfy the following mechanical stability criteria [25].

$$\begin{aligned} C_{11} > 0; C_{22} > 0; C_{33} > 0; C_{44} > 0; C_{55} > 0; C_{66} > 0; \\ [C_{11} + C_{22} + C_{33} + 2(C_{12} + C_{13} + C_{23})] > 0; \\ (C_{11} + C_{22} - 2C_{12}) > 0; (C_{11} + C_{33} - 2C_{13}) > 0; \\ (C_{22} + C_{33} - 2C_{23}) > 0; \end{aligned} \quad (13)$$

In fact, one can see from Table III that the calculated  $C_{12}$ ,  $C_{23}$ , and  $C_{13}$  are largely smaller than  $C_{11}$ ,  $C_{22}$ , and  $C_{33}$ . Therefore, the mechanical stability criteria is easily satisfied; (ii) Although the equilibrium volume of cotunnite-type  $\text{ThO}_2$  is distinctly compressed, its bulk modulus, shear modulus, and Young's modulus are all smaller by approximately 25% than those in fluorite-type  $\text{ThO}_2$ . This intriguing behavior has also been observed in the  $\text{UO}_2$  system [26], which, like  $\text{ThO}_2$ , will undergo a Fm3m  $\rightarrow$  Pnm phase transition. Since the 5f orbital band is occupied in  $\text{UO}_2$ , while it is almost empty in  $\text{ThO}_2$ , thus this similarity of the softening in moduli upon phase transition for the two systems is clearly unrelated with the 5f orbitals. From this aspect, we

speculate that most actinide dioxides share this phase-transition involved similarity. Again, we have confirmed for the Pnm phase that the bulk modulus  $B$  calculated by fitting the Murnaghan equation of state equals to that through VRH approximation; (iii) The Poisson's ratio of  $\text{ThO}_2$  in Pnm phase is nearly the same as in Fm3m phase, i.e., close to 1/3. This is understandable since the shear modulus is much smaller than the bulk modulus in the both two phases.

Now let us see the phase transition energetics of  $\text{ThO}_2$ . The total energies (per unit cell) of the two phases at different volumes are calculated and shown in Fig. 6. Obviously, the Fm3m phase is stable under ambient pressure while under high pressure the Pnm phase becomes stable. According to the rule of common tangent of two energy curves, a phase transition at 26.5 GPa is predicted by the slope shown in the inset of Fig. 6. Besides, we also determine the phase transition pressure by comparing the Gibbs free energy as a function of pressure. At 0 K, the Gibbs free energy is equal to the enthalpy  $H$ , expressed as  $H = E + PV$ . Figure 7 shows the relative enthalpies of the cotunnite phase with respect to the fluorite phase as a function of pressure. The crossing between the two enthalpy curves in Fig. 7 readily gives phase transition pressure of 26.5 GPa, which is fully consistent with the above result in terms of the common tangent rule. This value is well close to the experimental measurement by Idiri et al. [1] and by Jayaraman et al. [2] as 30 GPa. Here, the minor theoretical underestimation by 5.0 GPa is speculated to be caused by the possible existence of an energy barrier with an amplitude of  $\sim 0.06$  eV. To overcome this energy barrier, the external pressure  $P^0$  should be larger than the conventional common-tangent-rule determined pressure  $P$  by an amount  $P = P^0 + P$ . According to the experimentally measured transition pressure  $P^0$  [1] and our theoretically obtained common tangent curve in Fig. 6, we deduce the energy barrier amplitude to be 0.06 eV (per formula unit). This value is too small to survive the Pnm phase to ambient conditions, which is consistent with the fact that to date, the Pnm phase of  $\text{ThO}_2$  has only been observed under high pressures.

Figure 8 shows the relative volume  $V/V_0$  evolution with pressure for  $\text{ThO}_2$  in both Fm3m and Pnm phases. For comparison, the experimental data are also shown in the figure. Clearly, our calculated  $P$ - $V$  equation of state is well consistent with the experimental measurement for the both two phases of  $\text{ThO}_2$ . Specially, at the calculated transition pressure (26.5 GPa), our result in Fig. 8 gives that the volume collapse upon phase transition is 5.9%. This value is very close to the experimental data of 6.1% [1] with a little bit underestimation, which is obviously within the accuracy of GGA. Note that unlike the cubic Fm3m phase, in which all coordinates are completely determined at each volume due to the symmetry, the orthorhombic Pnm phase at each volume has two additional internal degrees of freedom that must be fully relaxed to obtain the energy minimum. Thus, we have further calculated and plotted in Fig. 9 the pressure de-

TABLE III: Calculated elastic constants, bulk modulus  $B$ , pressure derivative of the bulk modulus  $B'$ , shear modulus  $G$ , Young's modulus  $E$ , Poisson's ratio for cotunnite-type  $\text{ThO}_2$  at 0 GPa. Except the Poisson's ratio, all other values are in units of GPa.

$C_{11}$	$C_{22}$	$C_{33}$	$C_{44}$	$C_{55}$	$C_{66}$	$C_{12}$	$C_{23}$	$C_{13}$	$B$	$B'$	$G$	$E$	Poisson's ratio
299.3	256.3	235.6	37.4	54.9	84.9	73.7	95.5	104.8	148	7.8	65.9	172.2	0.307

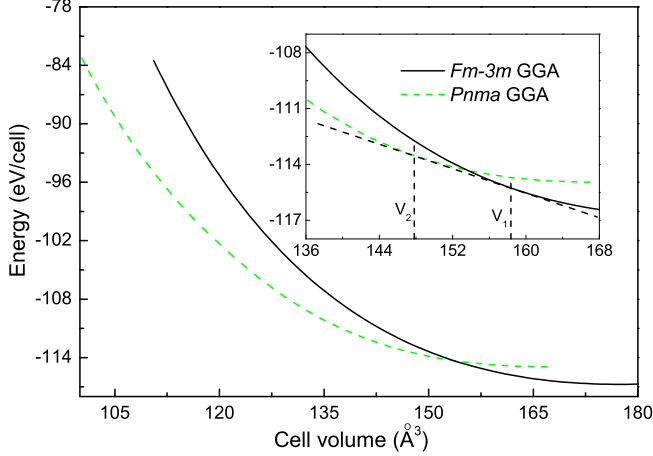


FIG. 6: (Color online) Comparison of total energy vs the cell volume for  $\text{ThO}_2$  in Fm-3m and Pnma phases. A phase transition at 26.5 GPa is predicted by the slope of the common tangent rule, as shown in the inset.

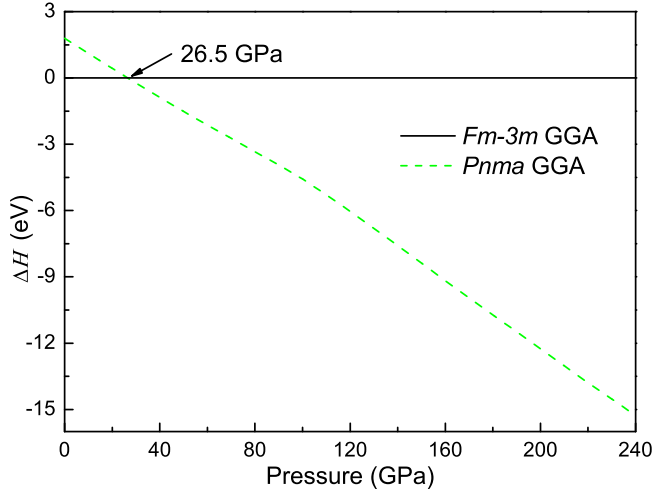


FIG. 7: (Color online) Calculated enthalpy differences of Pnma phase with respect to Fm-3m phase as a function of pressure.

pendence of the three lattice parameters (with respect to their equilibrium values) for the Pnma phase of  $\text{ThO}_2$ . In the experimentally reported pressure range from 30 GPa to 80 GPa, our calculated evolution of the relative lattice parameters in the Pnma phase are well consistent

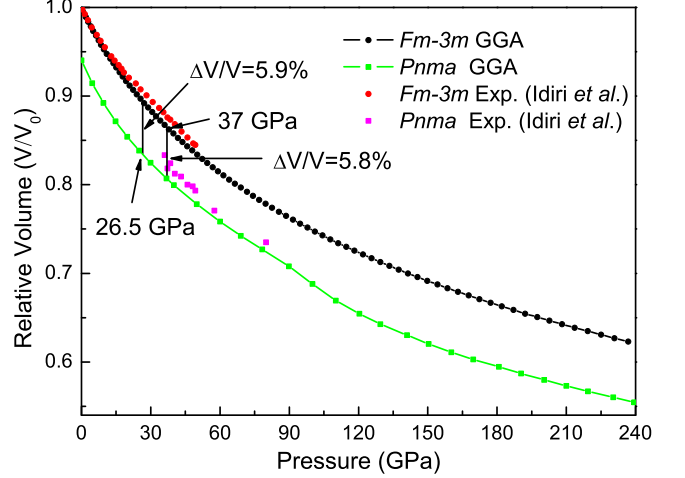


FIG. 8: (Color online) Calculated compression curves of  $\text{ThO}_2$  compared with experimental measurements. The volume collapses at our predicted phase transition point 26.5 GPa and experimental phase transition pressure 37 GPa are labeled.

with the experimental observation [1]. In this pressure region, one can see from Fig. 9 that the responses of the three relative lattice parameters to the compression are anisotropic in the sense that the compression of the middle axis  $a$  is most rapid compared to those of the long axis  $c$  and small axis  $b$ , which vary upon compression almost in the same tendency. When the pressure becomes higher to be between 80 and 130 GPa, remarkably, it reveals in Fig. 9 that all the three relative lattice parameters undergo dramatic variations by the fact that the small axis  $b$  has a strong rebound and the middle  $a$  is collapsed. When the pressure is beyond 130 GPa, then the variations of the three relative lattice parameters become smooth and approach isotropic compression. This signifies a typical isostructural transition for the Pnma phase of  $\text{ThO}_2$ . It should be stressed that this isostructural transition is not unique for  $\text{ThO}_2$ . Similar phenomenon has also been observed in other actinide dioxides [26].

To see the change of electronic structure of  $\text{ThO}_2$  under high pressure, we present in Fig. 10 the orbital-resolved PDOS for the Fm-3m and Pnma phases at the theoretical transition pressure of 26.5 GPa. One can see that there occurs an understandable narrowing in the band gap (4.6 eV for the Fm-3m phase and 3.15 eV for the Pnma phase). The valence and conduction bands carry a sizeable downward shift to stabilize the high-pressure Pnma



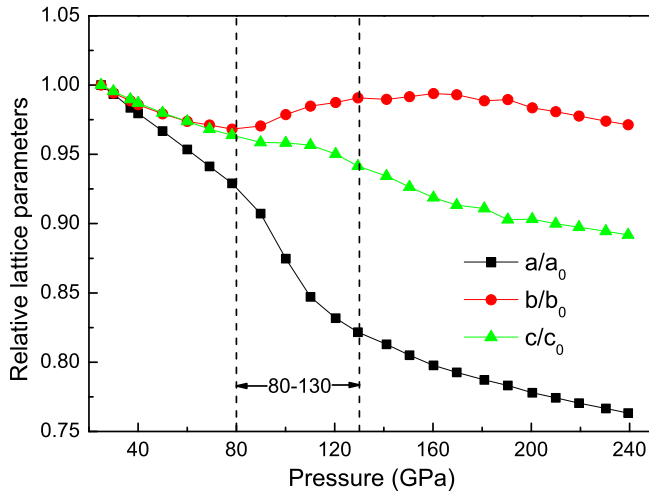


FIG. 9: (Color online) Pressure behavior of the relative lattice parameters of the  $Pnma$  phase, where the drastic change in the relative lattice constants (region between dashed lines) indicates an isostructural transition.

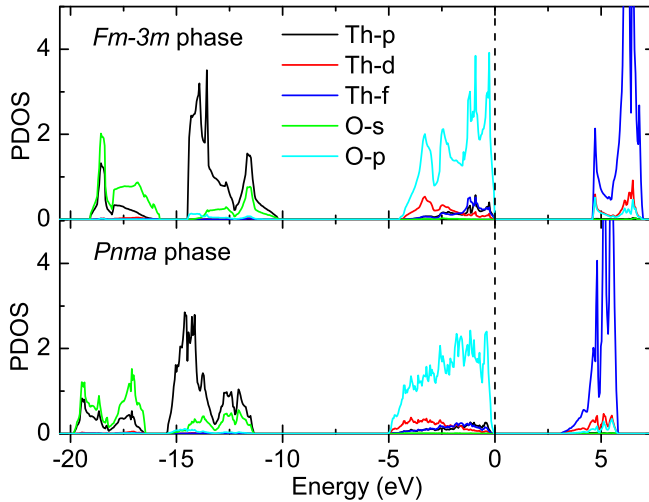


FIG. 10: (Color online) Partial density of states (PDOS) for  $Fm\bar{3}m$  phase (a) and  $Pnma$  phase (b) both at 26.5 GPa. The Fermi energy level is zero. The energy gaps of  $Fm\bar{3}m$  phase and  $Pnma$  phase are 4.584 eV and 3.153 eV, respectively.

phase. In addition, the valence and conduction bands are more widened and smooth in the  $Pnma$  phase. However, these changes in the electronic structure are trivial and thus cannot be associated with the exotic transition-accompanied volume collapse in  $ThO_2$  and other actinide dioxides. Concerning the 5f electron effect, here we would like to present our viewpoint as follows. First, the 5f orbital is almost empty for both two phases of  $ThO_2$ .

Therefore, the transition-accompanied volume collapse in  $ThO_2$  is irrelevant to the 5f orbital effect. Second, in other actinide dioxides, such as  $PuO_2$ , although taking into account the 5f electronic interaction is crucial to obtain more reasonable ground state [27], this local correlation effect is not expected to play a role in explaining the transition-accompanied volume collapse in these 5f-occupied actinide dioxides. The reason is simply because that inclusion of 5f electronic localization will weaken the binding of cations and anions, causing an increase instead of a decrease in the volume of system. Therefore, the phenomenon of volume collapse during high-pressure phase transition of the actinide dioxides is mainly attributed to the ionic (instead of electronic) response to the external compression.

## V. CONCLUSION

In summary, the ground state properties as well as the high pressure behavior of  $ThO_2$  were studied by means of the first-principles DFT-GGA method. The elastic constants and their derived moduli and Poisson's ratio were calculated for both the ambient  $Fm\bar{3}m$  and the high-pressure  $Pnma$  phases of  $ThO_2$  and were shown to accord well with recent reliable experiments. Based on these results, mechanical stability of the  $Pnma$  phase at zero pressure was predicted. The hardness, lattice vibration dynamics, and the Th-O chemical bond of the ambient phase were calculated and analyzed in order to support the practical application of  $ThO_2$ . We showed that the Th-O bond displays a mixed ionic/covalent character, with the valence of Th and O ions represented as  $Th^{3.834+}$  and  $O^{0.452-}$ . Here the ionicity is mainly featured by charge transfer from Th 6d=5f states to O 2p states, while the covalency is manifested by hybridization of oxygen 2s and thorium 6p states. This mixed ionic/covalent feature makes  $ThO_2$  a hard material, with its hardness calculated in this paper to be 27 GPa. As another main task, we studied phase transition of  $ThO_2$  under high pressure. Our calculated  $Fm\bar{3}m \rightarrow Pnma$  transition pressure is 26.5 GPa, according well with recent experimental results of 30 GPa. Our calculated transition-accompanied volume collapse of 5.9% is also in good agreement with the experimental data of 6.1%. Under more higher pressure, we further found that there occurred an isostructural transition between 80 and 130 GPa for the  $Pnma$  phase, which is to be experimentally verified in future.

## Acknowledgments

This work was supported by the Grant Agency of the Chinese Academy of Engineering Physics.

[1] M. Idiri, M. T. Le Bihan, S. Heathman, and J. Rebizant, Phys. Rev. B 70, 014113 (2004).

[2] A. Jayaraman, G. A. Kourouklis, and L. G. Van Uitert,



- Pramana* 30, 225 (1988).
- [3] J. P. Dancus, E. Gering, S. Heathman, and U. Benedict, *High Press. Res.* 2, 381 (1990).
  - [4] P. J. Kelly and M. S. S. Brooks, *J. Chem. Soc., Faraday Trans. 2* 83, 1189 (1987).
  - [5] J. H. Harding, P. J. D. Lindan, and N. C. Pyper, *J. Phys.: Condens. Matter* 6, 6485 (1994).
  - [6] J. Staun Olsen, L. Gerward, V. Kanchana, and G. Vaitheeswaran, *J. Alloys Compounds* 381, 37 (2004).
  - [7] S. Li, R. Ahuja, and B. Johansson, *High Press. Res.* 22, 471 (2002).
  - [8] V. Kanchana, G. Vaitheeswaran, A. Svane, and A. Delin, *J. Phys.: Condens. Matter* 18, 9615 (2006).
  - [9] G. Kresse and J. Furthmüller, *Phys. Rev. B* 54, 11169 (1996).
  - [10] J. P. Perdew, K. Burke, and Y. Wang, *Phys. Rev. B* 54, 16533 (1996).
  - [11] P. E. Blochl, *Phys. Rev. B* 50, 17953 (1994).
  - [12] H. J. Monkhorst and J. D. Pack, *Phys. Rev. B* 13, 5188 (1972).
  - [13] F. Birch, *Phys. Rev.* 71, 809 (1947).
  - [14] J. F. Nye, *Physical Properties of Crystals, Their Representation by Tensors and Matrices* (Oxford Press, 1957), Chap V III.
  - [15] *Intermetallic Compounds: Principles and Practice, Vol I: principles*, edited by J. H. Westbrook and R. L. Fleischer (Wiley, London, 1995), Chap. 9 pp. 195-210.
  - [16] P. M. Macedo, W. Capps, and J. B. Wachtman, *J. Am. Ceram. Soc.* 47, 651 (1964).
  - [17] W. Voigt, *Lehrbuch der Kristallphysik* (Teubner, Leipzig, 1928).
  - [18] A. Reuss and Z. Angew, *Math. Mech.* 9, 49 (1929).
  - [19] R. Hill, *Phys. Soc. London* 65, 350 (1952).
  - [20] J. P. Watt, *J. Appl. Phys.* 50, 6290 (1979).
  - [21] P. Ravindran, L. Fast, P. A. Korzhavyi, B. Johansson, J. Wills, and O. Eriksson, *J. Appl. Phys.* 84, 4891 (1998).
  - [22] A. Simunek and J. Vackar, *Phys. Rev. Lett.* 96, 085501 (2006).
  - [23] A. A. Sviridova, and N. V. Suikovskaya, *Opt. Spectrosc.* 22, 940 (1965).
  - [24] B. Wang, P. Zhang, H. Shi, B. Sun, and W. Li, *arXiv:0905.4589v1 [cond-mat.mtrl-sci]* (2009).
  - [25] J. F. Nye, *Physical Properties of Crystals* (Oxford University Press, 1985).
  - [26] H. Y. Geng, Y. Chen, Y. Kaneta, and M. K. Inoshita, *Phys. Rev. B* 75, 054111 (2007).
  - [27] B. Sun, P. Zhang, and X.-G. Zhao, *J. Chem. Phys.* 128, 084705 (2008).